1 **SARS-CoV-2 RNA quantification using droplet digital RT-PCR**

2

3 Natalie N. Kinloch[1,2], Gordon Ritchie[3,4], Winnie Dong[2], Kyle D. Cobarrubias[2], Hanwei
4 Sudderuddin[2], Tanya Lawson[3], Nancy Matic[3,4], Julio S.G. Montaner[2,5], Victor Leung[3,4,5], Marc
5 G. Romney[3,4], Christopher F. Lowe[3,4], Chanson J. Brumme[2,5#], Zabrina L. Brumme[1,2#]

6

7 [#]denotes equal contribution

8

9 [1]Faculty of Health Sciences, Simon Fraser University, Burnaby, British Columbia, Canada
10 [2]British Columbia Centre for Excellence in HIV/AIDS, Vancouver, British Columbia, Canada
11 [3]Division of Medical Microbiology and Virology, St Paul's Hospital, Vancouver, British
12 Columbia, Canada
13 [4]Department of Pathology and Laboratory Medicine, University of British Columbia, Vancouver,
14 British Columbia, Canada
15 [5]Department of Medicine, University of British Columbia, Vancouver, British Columbia, Canada

16

17 Running Title: SARS-CoV-2 RNA quantification using RT-ddPCR

18

19 Keywords: SARS-CoV-2; RT-ddPCR; ddPCR; viral load; quantification; COVID-19

20

21 Correspondent Footnote:

22

23 Zabrina L. Brumme, Ph.D.
24 Professor, Faculty of Health Sciences
25 Simon Fraser University
26 8888 University Drive
27 Burnaby, BC, Canada
28 V5A 1S6
29 778-782-8872
30 zbrumme@sfu.ca

31

32 Chanson J. Brumme, Ph.D.
33 Assistant Professor, Faculty of Medicine
34 University of British Columbia
35 675-1081 Burrard Street, St. Paul's Hospital
36 Vancouver, BC
37 V6Z 1Y6
38 604-682-2344 ext. 63211
39 cbrumme@bccfe.ca

40

41

42

43

Abstract

Quantitative viral load assays have transformed our understanding of − and ability to manage − viral diseases. They hold similar potential to advance COVID-19 control and prevention, but SARS-CoV-2 viral load tests are not yet widely available. SARS-CoV-2 molecular diagnostic tests, which typically employ real-time reverse transcriptase-polymerase chain reaction (RT-PCR), yield semi-quantitative results only. Reverse transcriptase droplet digital PCR (RT-ddPCR), a technology that partitions each reaction into 20,000 nanolitre-sized droplets prior to amplification, offers an attractive platform for SARS-CoV-2 RNA quantification. We evaluated eight primer/probe sets originally developed for real-time RT-PCR-based SARS-CoV-2 diagnostic tests for use in RT-ddPCR, and identified three (Charité-Berlin E-Sarbeco and Pasteur Institute IP2 and IP4) as the most efficient, precise and sensitive for RT-ddPCR-based SARS-CoV-2 RNA quantification. Analytical efficiency of the E-Sarbeco primer/probe set, for example, was ~83%, while assay precision, as measured by the coefficient of variation, was ~2% at 1000 input copies/reaction. Lower limits of quantification and detection for this primer/probe set were 18.6 and 4.4 input SARS-CoV-2 RNA copies/reaction, respectively. SARS-CoV-2 RNA viral loads in a convenience panel of 48 COVID-19-positive diagnostic specimens spanned a 6.2$\log_{10}$ range, confirming substantial viral load variation *in vivo*. We further calibrated RT-ddPCR-derived SARS-CoV-2 E gene copy numbers against cycle threshold (C_t) values from a commercial real-time RT-PCR diagnostic platform. The resulting log-linear relationship can be used to mathematically derive SARS-CoV-2 RNA copy numbers from C_t values, allowing the wealth of available diagnostic test data to be harnessed to address foundational questions in SARS-CoV-2 biology.

69 **Introduction**
70
71   Quantitative viral load assays have revolutionized our ability to manage viral diseases (1-

72   6). While not yet widely available for SARS-CoV-2, quantitative assays could advance our

73   understanding of COVID-19 biology and inform infection prevention and control measures (7,

74   8). Most SARS-CoV-2 molecular diagnostic assays however, which use real-time reverse

75   transcriptase PCR (RT-PCR) to detect one or more SARS-CoV-2 genomic targets using

76   sequence-specific primers coupled with a fluorescent probe, are only semi-quantitative. These

77   tests produce cycle threshold (C_t) values as readouts, which represent the PCR cycle where the

78   sample began to produce fluorescent signal above background. While each C_t value decrement

79   corresponds to a roughly two-fold higher viral load (due to the exponential nature of PCR

80   amplification), C_t values cannot be directly interpreted as SARS-CoV-2 viral loads without

81   calibration to a quantitative standard (9). Rather, C_t values are interpreted as positive,

82   indeterminate or negative based on assay-specific cutoffs and evolving clinical guidelines. Due

83   to differences in nucleic acid extraction method, viral target and other parameters, C_t values are

84   also not directly comparable across assays or technology platforms.

85   Reverse transcriptase droplet digital PCR (RT-ddPCR) offers an attractive platform for

86   SARS-CoV-2 RNA quantification (10, 11). Like real-time RT-PCR, ddPCR employs target-

87   specific primers coupled with a fluorescent probe, making it relatively straightforward to adapt

88   assays. In ddPCR however, each reaction is fractionated into 20,000 nanolitre-sized droplets

89   prior to massively parallel PCR amplification. At end-point, each droplet is categorized as

90   positive (target present) or negative (target absent), allowing for absolute target quantification

91   using Poisson statistics. This sensitive and versatile technology has been used for mutation

92   detection and copy number determination in the human genome (12), target verification

93   following genome editing (13), and copy number quantification for viral pathogens (14-19).

94   Several real-time RT-PCR SARS-CoV-2-specific primer/probe sets have been used in RT-

95   ddPCR (10, 11, 20-22) with results achieving high sensitivity in some reports (11, 21, 23-25), but

96   few studies have rigorously evaluated SARS-CoV-2-specific primer/probe set performance in

97   RT-ddPCR using RNA as a template. Furthermore, no studies to our knowledge have calibrated

98   SARS-CoV-2 viral loads to diagnostic test C_t values. Here, we evaluate eight SARS-CoV-2-

99   specific primer/probe sets originally developed for real-time RT-PCR (26), for use in RT-

100   ddPCR. We also derive a linear equation relating RT-ddPCR-derived SARS-CoV-2 viral loads

101   and real-time RT-PCR-derived C_t values for a commercial diagnostic assay, the LightMix®

102   Modular SARS-CoV (COVID19) E-gene assay, allowing conversion of existing COVID-19

103   diagnostic results to viral loads.

104   **Materials and Methods**

105

106   **Primer and Probe Sets**

107   Eight SARS-CoV-2-specific primer/probe sets developed for real-time RT-PCR COVID-

108   19 diagnostic assays (26) were assessed for use in RT-ddPCR (Table 1). These included the

109   Charité-Berlin E gene ('E-Sarbeco') set (27), the Pasteur Institute RdRp IP2 and IP4 sets ('IP2'

110   and 'IP4', respectively) (28), the Chinese Centre for Disease Control ORF and N gene sets

111   ('China-ORF' and 'China-N', respectively) (29), the Hong Kong University ORF and N gene

112   sets ('HKU-ORF' and 'HKU-N', respectively) (30), and the US-CDC-N1 set (31).

113   **SARS-CoV-2 Synthetic RNA standards**

114   RT-ddPCR assays were evaluated using commercial synthetic SARS-CoV-2 RNA

115   standards comprising six non-overlapping 5,000 base fragments of equal quantities encoding the

116   Wuhan-Hu-1 SARS-CoV-2 genome (Control 2, Genbank ID MN908947.3; Twist Biosciences,

117   supplied at approximately 1 million copies/fragment/μl). To avoid degradation, RNA standards

118   were stored at -80°C and thawed only once, immediately before use, to perform the analytical

119   efficiency, precision, analytical sensitivity and dynamic range analyses described herein.

120   Moreover, to mimic nucleic acid composition of a real biological specimen, all assays employing

121   these standards were supplemented with a consistent, physiologically relevant amount of nucleic

122   acid extracted from pooled remnant SARS-CoV-2-negative nasopharyngeal swabs

123   (Supplementary Figure 1). Briefly, pooled viral transport medium was extracted in 1ml aliquots

124   on the BioMerieux NucliSens® EasyMag®, eluted in 60μl and re-pooled. The resulting material

125   contained DNA from on average 2,200 human cells/μl (as quantified using human RPP30 DNA

126   copy numbers by ddPCR as described in (32)) and 4,400 human RNAse P copies/μl extract (as

127   quantified by RT-ddPCR as described in (33)), concentrations that are in line with human DNA

128   and RNA levels recovered on nasopharyngeal swabs (32, 33).

129   **Reverse transcriptase droplet digital PCR (RT-ddPCR) for SARS-CoV-2 quantification**

130

131   RT-ddPCR reactions were performed by combining relevant SARS-CoV-2 RNA

132   template with target-specific primers and probe (900nM and 250nM, respectively, Integrated

133   DNA Technologies; Table 1), One-Step RT-ddPCR Advanced Kit for Probes Supermix, Reverse

134   Transcriptase and DTT (300nM) (all from BioRad), XhoI restriction enzyme (New England

135   Biolabs), background nucleic acid (for reactions employing synthetic RNA template only, see

136   above) and nuclease free water. Droplets were generated using an Automated Droplet Generator

137   (BioRad) and cycled under primer/probe set-specific conditions (see below and Figure 1).

138   Analysis was performed on a QX200 Droplet Reader (BioRad) using QuantaSoft software

139   (BioRad, version 1.7.4).

140   **Thermal cycling temperature optimization**

141   For each primer/probe set, acceptable thermal cycling temperature ranges for reverse

142   transcription (RT) and PCR annealing/extension were determined by modifying the

143   manufacturer-recommended default conditions, which are 42-50°C for 1 hour (for reverse

144   transcription); 95°C for 10 minutes; 40 cycles of (94°C for 30 seconds followed by 50-63°C for

145   1 minute); 98°C for 10 minutes and 4°C infinite hold. To determine acceptable temperature

146   ranges for reverse transcription, a thermal gradient from 42-51.5°C was performed while fixing

147   the annealing/extension step at 52°C. Using the optimized reverse transcription temperature, a

148   thermal gradient from 50-63°C was then performed to identify acceptable annealing/extension

149   temperature ranges. Temperatures that produced insufficient separation of positive from negative

150   droplets or non-specific amplification were deemed unacceptable, as were those that produced

151   consecutive 95% confidence intervals of copy number estimates outside those of the maximal

152   point-estimate.

Analytical Efficiency and Precision

154   The analytical efficiency of each primer/probe set to quantify SARS-CoV-2 RNA by RT-

155   ddPCR was determined using synthetic SARS-CoV-2 RNA standards at 1000 and 100 input

156   copies. A minimum of three (maximum four) technical replicates were performed at each

157   concentration. Analytical efficiency was calculated by dividing the measured SARS-CoV-2 copy

158   number by the expected input copy number, and multiplying by 100. Precision was expressed as

159   the coefficient of variation (CV), expressed as a percentage, across technical replicates.

Linear Dynamic Range

161   The linear dynamic range (LDR) of each primer/probe set of interest was determined

162   across a serial 1:2 dilution series from 114,286 to 1.2 SARS-CoV-2 RNA copies/reaction. This

163   range of concentrations was chosen as it crosses the entire range of recommended input copies

164   for a ddPCR reaction seeking to quantify the target of interest (34). Reactions were performed in

165   duplicate. The upper and lower limits of quantification of (ULOQ and LLOQ, respectively) were

166   defined as the upper and lower boundaries of the concentration range over which the relationship

167   between measured and input SARS-CoV-2 RNA copies was linear. This was determined by

168   iteratively restricting the range of concentrations included in the linear regression of measured

169   versus input SARS-CoV-2 RNA copies to identify that which maximized the coefficient of

170   determination (R^2) value and minimized the residuals.

Assay Analytical Sensitivity

172   Assay analytical sensitivity, defined as the Lower Limit of Detection (LLOD), was

173   determined for primer/probe sets of interest by serially diluting synthetic SARS-CoV-2 RNA

174 standards to between 47.6 and 0.74 SARS-CoV-2 RNA copies/reaction. Between 6 and 18

175 technical replicates were performed for each dilution and results were analyzed using probit

176 regression. The LLOD, determined through interpolation of the probit curve, was defined as the

177 concentration of input SARS-CoV-2 RNA in a reaction where the probability of detection was

178 95%.

179 **SARS-CoV-2 RNA quantification in biological specimens, and relationship to C_t value**

180   Optimized RT-ddPCR assays were applied to a convenience sample of 48 consecutive

181 remnant SARS-CoV-2-positive diagnostic nasopharyngeal swab specimens that were originally

182 submitted to the St. Paul's Hospital Virology Laboratory in Vancouver, Canada for diagnostic

183 testing using the Roche cobas® SARS-CoV-2 assay. For these samples, total nucleic acids were

184 re-extracted from 250µl remnant media using the BioMerieux NucliSens® EasyMag® and

185 eluted in 50µl. Eluates were aliquoted and frozen at -80°C prior to single use. SARS-CoV-2 copy

186 numbers were quantified by RT-ddPCR as described above. As our main goal was to

187 characterize the relationship between C_t values and SARS-CoV-2 RNA levels without

188 confounding by extraction platform, quantity of input material or SARS-CoV-2 genomic target,

189 we re-tested these extracts using a commercial real-time RT-PCR SARS-CoV-2 diagnostic assay

190 that uses the E-Sarbeco primer/probe set (27): the LightMix® 2019-nCoV real-time RT-PCR

191 assay E-gene target (Tib-Molbiol), implemented on LightCycler 480 (Roche Diagnostics).

192 Finally, to be responsive to a recent recommendation that SARS-CoV-2 viral loads be reported

193 in terms of SARS-CoV-2 RNA copies per human cell equivalents (9), we measured human

194 cells/µl extract by ddPCR as previously described (32) and additionally reported results as

195 SARS-CoV-2 RNA copies/1,000 human cells.

196 **Statistical Analysis**

8

197   Statistical analysis was performed using GraphPad Prism (Version 8) or Microsoft Excel

198   (Version 14.7.2).

199   **Ethical Approval**

200   This study was approved by the Providence Health Care/University of British Columbia

201   and Simon Fraser University Research Ethics Boards under protocol H20-01055.

202

Results

Thermal cycling optimization for SARS-CoV-2 quantification by RT-ddPCR

203

204

205   Eight primer/probe sets originally developed for SARS-CoV-2 diagnostic testing by real

206   time RT-PCR were evaluated for use in RT-ddPCR (Table 1). As these primer/probe sets vary in

207   sequence, amplicon length and SARS-CoV-2 genomic target, we first determined the acceptable

208   temperature ranges for reverse transcription (RT) and PCR annealing/extension. Most

209   primer/probe sets were tolerant to a wide temperature range, and background signal was

210   essentially zero at all temperatures tested (Figure 1). The E-Sarbeco primer/probe set for

211   example produced consistent amplitude profiles, copy number estimates and essentially zero

212   background at annealing/extension temperatures ranging from 50-63°C (Figure 1A and data not

213   shown). The HKU-ORF primer/probe performed acceptably over a 50-60.5°C

214   annealing/extension range, but positive and negative droplet separation was insufficient at higher

215   temperatures (Figure 1B). Acceptable temperature ranges for each primer/probe set are shown in

216   Figure 1C. All subsequent experiments were performed at RT 42.7°C and annealing/extension

217   50.9°C except those for HKU-ORF and US-CDC-N1, which were performed at RT 45.7°C and

218   annealing/extension 55.1°C as informed by initial qualitative assessments.

Analytical Efficiency and Precision of SARS-CoV-2 quantification by RT-ddPCR

219

220   We next evaluated the analytical efficiency of SARS-CoV-2 RNA quantification for each

221   primer/probe set, calculated as the percentage of input viral RNA copies detected by the assay.

222   We also evaluated precision, calculated as the dispersion of measured copies around the mean

223   (coefficient of variation, CV). Analytical efficiency and precision were evaluated at 1000 and

224   100 SARS-CoV-2 RNA target input copies. At 1000 input copies, primer/probe set analytical

225   efficiency ranged from 83% (E-Sarbeco) to 15% (US-CDC-N1) (Figure 2A). At 100 copies, the

10

226   analytical efficiency hierarchy was identical, with values ranging from 74% (E Sarbeco) to 12%

227   (US-CDC-N1). Of all primer/probe sets evaluated, the E-Sarbeco, IP2 and IP4 sets had the

228   highest analytical efficiencies by a substantial margin. At 1000 and 100 target copies, E-Sarbeco

229   analytical efficiency was 83% (95% Total Poisson Confidence Interval [CI]: 79- 87%) and 74%

230   (95% CI: 63- 84%), respectively; IP2, analytical efficiency was 70% (95% CI: 67- 73%) and

231   55% (95% CI: 46- 64%), respectively; and IP4 analytical efficiency was 69% (95% CI: 66- 72%)

232   and 59% (95% CI: 50-69%), respectively. In contrast, analytical efficiency of the China-ORF

233   primer/probe set was only 46% and 39% at 1000 and 100 input copies, respectively, and the

234   analytical efficiencies of the remaining sets were less than 30% regardless of input copy number.

235   Furthermore, while measurement precision generally decreased at the lower template

236   concentration (35), the E-Sarbeco, IP2 and IP4 primer/probe sets were nevertheless among the

237   most precise, with coefficients of variation (CV) of less than 5% at 1,000 input copies and less

238   than 15% at 100 input copies (Figure 2B). Combined analytical efficiency and precision data

239   confirmed E-Sarbeco, IP2 and IP4 as the best-performing primer/probe sets in RT-ddPCR

240   (Figures 2C and 2D), so these were moved forward for further characterization.

241   **Reduced analytical efficiency when IP2 and IP4 are duplexed in RT-ddPCR**

242   As IP2 and IP4 were originally designed for duplexing in real-time RT-PCR (28), we

243   evaluated them in duplex for RT-ddPCR. Duplexing however decreased analytical efficiency,

244   from 70% to 52% (at 1000 input copies) and 55% to 37% (at 100 input copies) for IP2, and from

245   69% to 49% (at 1000 input copies) and 59% to 38% (at 100 input copies) for IP4 (Supplemental

246   Figure 2A). Duplexing also decreased precision (Supplemental Figure 2B). For IP2, CV

247   increased from 5% to 11% when duplexing at 1000 input copies, and from 15% to 25% when

248   duplexing at 100 input copies. For IP4, CV increased from 4% to 7% (1000 input copies) and

249   from 14% to 21% (100 input copies) with duplexing. Duplexing of these reactions is therefore

250   not recommended in RT-ddPCR, and all IP2 and IP4 assays were performed as single reactions.

251   **Linear Dynamic Range and Limits of Quantification of SARS-CoV-2 RNA by RT-ddPCR**

252   Droplet digital PCR can achieve absolute target copy number quantification without a

253   standard curve. To investigate the linear dynamic range (LDR) of quantification of the E-

254   Sarbeco, IP2 and IP4 assays, we set up 18 two-fold serial dilutions of synthetic SARS-CoV-2

255   RNA beginning at 114,286 copies/reaction (this copy number is obtained when 120,000 copies

256   are added to a 21μl reaction, of which 20μl is used for droplet generation) and ending with 2.32

257   copies/reaction. This input copy number range crosses nearly the entire manufacturer-

258   recommended template input range for ddPCR reactions seeking to quantify the target of interest,

259   which is 1- 100,000 copies/reaction (36).

260   The LDR of each assay was determined by iteratively restricting the range of

261   concentrations included in the linear regression of measured versus input SARS-CoV-2 RNA

262   copies to identify the range that maximized the R^2 value and minimized the residuals. For E-

263   Sarbeco, the regression spanning 18.6-114,286 input SARS-CoV-2 RNA copies per reaction, an

264   approximately 6,100-fold concentration range, yielded an R^2 value of 0.9995 (Figure 3A, left).

265   Restricting the linear regression to this range also minimized the residuals of all included data

266   points to ±0.065$\log_{10}$ copies/reaction (Figure 3A, right). The IP2 assay, while less efficient than

267   E-Sarbeco, had the same estimated LDR of 18.6-114,286 input copies/reaction (Figure 3B, left).

268   This produced an R^2 value of 0.9995 and residuals within ±0.065$\log_{10}$ copies/reaction across the

269   LDR (Figure 3B, right). The LDR of IP4 was estimated as 37.2- 114,286 input copies/reaction,

270   an approximately 3,000-fold range, which yielded an R^2= 0.9975 and produced residuals within

271   ±0.11$\log_{10}$ copies/reaction across this range (Figure 3C). For all three assays, 114,286 input

272   copies/reaction should be considered a conservative estimate of the upper limit of quantification,

273   as saturation of the RT-ddPCR reaction or loss of linearity was still not achieved at this

274   concentration.

275   **Lower Limit of Detection of SARS-CoV-2 RNA by RT-ddPCR**

276   We next determined the lower limit of detection (LLOD) of the E-Sarbeco, IP2 and IP4

277   RT-ddPCR assays (Figure 4). Probit regression analysis applied to serial dilutions of synthetic

278   SARS-CoV-2 RNA standards revealed the E-Sarbeco RT-ddPCR assay to be the most

279   analytically sensitive of the three, which is consistent with it also having the highest analytical

280   efficiency. Specifically, the estimated LLOD of the E-Sarbeco assay was 4.4 (95% Confidence

281   Interval [CI]: 2.4-5.7) SARS-CoV-2 RNA copies/reaction (Figure 4A). The estimated LLOD of

282   the IP2 assay was 7.8 (95% CI: 4.4-10.3) SARS-CoV-2 RNA copies/reaction (Figure 4B), while

283   that of IP4 was 12.6 (95% CI: 6.9-16.5) SARS-CoV-2 RNA copies per reaction (Figure 4C).

284   **SARS-CoV-2 viral loads in biological samples**

285   SARS-CoV-2 viral loads were measured in 48 confirmed SARS-CoV-2 positive samples

286   using the E-Sarbeco, IP2 and IP4 primer/probe sets (note that samples with original diagnostic

287   test C_t values <19 required RNA extracts to be diluted up to 1:200 prior to quantification to

288   ensure that input copies measurements fell within each assay's LDR). The results revealed that

289   SARS-CoV-2 RNA in these biological samples varied over a 6.2 $\log_{10}$ range (Figure 5A).

290   Average copy numbers measured using the E-Sarbeco assay (which targets the E gene) were

291   higher than those using the IP2 and IP4 assays (which target ORF1a and ORF1b, respectively)

292   (Figure 5A). This is consistent with assay analytical efficiency (Figure 2) and *in vivo* coronavirus

293   RNA expression patterns, where transcripts covering the 3' end of the genome are more

294   abundant than those covering the 5' end (37-40). Specifically, the median E-gene copy number

295   was 5.1 (IQR 3.9- 5.7) $\log_{10}$copies/µl extract compared to a median of 4.9 (IQR 3.9- 5.5)

296    $\log_{10}$copies/µl extract for the IP2 target, and a median of 4.9 (IQR 3.9- 5.6) $\log_{10}$ copies/µl

297   extract for the IP4 target. SARS-CoV-2 E-gene, IP2 and IP4 copy numbers in biological samples

298   correlated strongly with one another (Spearman's ρ>0.99; p<0.0001 for all pairwise analyses;

299   Figure 5BCD). Consistent with comparable ORF1a and ORF1b RNA transcript levels *in vivo*

300   (37, 38, 40), IP2 and IP4 copy numbers were also highly concordant (Lin's concordance

301   correlation coefficient, ρc=0.9996 [95% CI: 0.9993- 0.9998]) (Figure 5D). Based on a recent

302   recommendation (9), we also report our results in terms of SARS-CoV-2 RNA copies per human

303   cell equivalents: results for E-Sarbeco spanned an 7-fold range from 1.05 to 7.3 $\log_{10}$SARS-

304   CoV-2 RNA copies/1,000 human cells, with IP2 and IP4 $\log_{10}$ copy numbers lower, as expected

305   (Supplemental Figure 3A). The Spearman's correlation between absolute and human cell-

306   normalized viral loads was strong (ρ=0.9717; p<0.0001; Supplementary Figure 3B), which is

307   consistent with the assumption that the amount of biological material collected by

308   nasopharyngeal swabs is relatively consistent.

309   **Inferring SARS-CoV-2 viral loads from diagnostic C_t values**

310   Finally, we characterized the relationship between C_t values produced by a commercial

311   COVID-19 diagnostic platform and SARS-CoV-2 RNA copy numbers. We selected the

312   LightMix® 2019-nCoV real-time RT-PCR assay, E-gene target (Tib-Molbiol), implemented on a

313   LightCycler 480 (Roche Diagnostics) because commercial diagnostic reagents comprising the E-

314   Sarbeco primer/probe set exist for this platform (27) and because it takes purified nucleic acids

315   as input, thereby allowing direct comparison of results from the same starting material (real-time

316   RT-PCR platforms that take biological material as input are suboptimal for such a comparison

317   because the onboard extraction introduces an additional variable). As the C_t values reported for

14

318   the LightMix® assay are based on a 9μl extract input volume, our primary analysis reported RT-

319   ddPCR results in terms of SARS-CoV-2 copies equivalent (*i.e.* SARS-CoV-2 copies in 9μl of

320   extract), to allow direct conversion of C_t values to absolute viral copy numbers.

321   Sample C_t values ranged from 11.34-31.18 (median 18.69 [IQR 16.73- 22.69]) using the

322   LightMix® assay. The relationship between C_t value and SARS-CoV-2 RNA copy numbers was

323   log-linear, with an $R^2 = 0.9990$ (Figure 6). Despite this strong relationship, inspection of the

324   residuals nevertheless suggested modest departures from log-linearity at the extremes of the

325   linear range (Supplementary Figure 4). The relationship between C_t value and absolute SARS-

326   CoV-2 E-gene copies can thus be given by $\log_{10}$SARS-CoV-2 E gene copies equivalent =

327    $-0.3038C_t +11.7$ (Figure 6). That is, a C_t value of 20 corresponds to 453,942 (*i.e.* 5.66 $\log_{10}$)

328   SARS-CoV-2 RNA copies, while a C_t value of 30 corresponds to 416 (*i.e.* 2.62 $\log_{10}$) viral

329   copies. This equation also predicts that the C_t values corresponding to the LLOQ and LLOD of

330   the E-Sarbeco RT-ddPCR assays are 34.8 and 36.84, respectively. When measured SARS-CoV-2

331   RNA copy numbers are expressed as human cell-normalized viral loads, the relationship with Ct

332   value is given by $\log_{10}$SARS-CoV-2 E gene copies/1,000 human cells = $-0.3041C_t + 10.8$

333   (Supplemental Figure 5). An extract that yielded a C_t value of 20 therefore is estimated to have

334   contained 48,978 (*i.e.* 4.69 $\log_{10}$) SARS-CoV-2 RNA copies/1,000 human cells, while one with

335   C_t value of 30 is estimated to have contained 45 (i.e. 1.66 $\log_{10}$) copies/1,000 human cells

336

337   **Discussion**

338   While real-time and droplet digital RT-PCR platforms both employ target-specific

339   primers coupled with fluorescence-based amplicon detection, there are key differences in

340   reaction chemistry (*e.g.* RT-ddPCR reagents must be compatible with water-in-oil droplet

15

341   partitioning) and probe chemistry (*e.g.* while real-time RT-PCR uses fluorescent quenchers,

342   ddPCR typically uses dark quenchers). As a result, assays developed for one platform may not

343   always translate seamlessly to the other. For example, ddPCR probes should ideally not have a

344   Guanine at their 5' end because this quenches the fluorescence signal even following hydrolysis

345   (36) but the HKU-N probe has a G at its 5' end (Table 1).

346   It is perhaps therefore not surprising that the overall performance of the eight

347   primer/probe sets in RT-ddPCR did not exactly mirror that in real-time RT-PCR (41, 42).

348   Nevertheless, E-Sarbeco, IP2 and IP4, which represented the most efficient and precise

349   primer/probe sets for SARS-CoV-2 RNA quantification by RT-ddPCR are also among the most

350   efficient in real-time RT-PCR (41, 42). Our results also confirm previous reports of the E-

351   Sarbeco primer/probe set performing well in RT-ddPCR (10, 22). Other primer/probe sets

352   however, notably US CDC-N1, HKU-ORF and China-ORF, did not perform as well in our RT-

353   ddPCR assay compared to a previous report (10). One key difference is that, while we used

354   sequence-specific reverse transcription (with the reverse primer) in a one-step RT-ddPCR

355   reaction, the previous study featured an independent reverse transcription reaction primed with

356   random hexamers and oligo dT, which can yield higher efficiency than sequence-specific

357   priming (35, 43-45), to generate cDNA for input into a ddPCR reaction. To our knowledge, ours

358   is the first study to evaluate IP2 or IP4 primer/probe sets in RT-ddPCR.

359   The analytical sensitivities of the RT-ddPCR assays reported here are nevertheless

360   comparable to existing estimates. The limit of detection of the BioRad SARS-CoV-2 ddPCR Kit

361   (20) is, for example, estimated at 150 copies/mL, which is comparable to our E-Sarbeco RT-

362   ddPCR assay (estimated at 75.8 copies/mL assuming 100% extraction efficiency). Similarly, the

363   LLODs of the TargetingOne (Beijing, China) COVID-19 digital PCR detection kit (23) and a

364   multiplex assay that included the E-Sarbeco primer/probe set (22) were reported at 10 copies/test

365   and 5 copies/reaction, respectively, both comparable to the LLOD determined here. While a

366   number of studies have reported that RT-ddPCR can detect SARS-CoV-2 RNA in low viral load

367   clinical samples with higher sensitivity than real-time RT-PCR (11, 21, 23-25), our study was

368   not designed to evaluate this. Our estimated LLOD of 4.4 copies/reaction by RT-ddPCR using

369   the E-Sarbeco primer/probe set (Figure 4) is in fact comparable to the LLOD reported for many

370   real-time RT-PCR-based COVID-19 diagnostic assays (46).

371   The ability to quantify SARS-CoV-2 viral loads in biological samples can advance our

372   understanding of COVID-19 biology, and RT-ddPCR offers an attractive platform (7, 8). Our

373   observation that, in a small convenience sample, both absolute and human cell-normalized (9)

374   SARS-CoV-2 loads spanned a more than 6 $\log_{10}$ range confirms an enormous viral load range *in*

375   *vivo* (47) and suggests that some of the high viral load samples measured here were from

376   individuals with early and progressive infection (23, 48-50) or who were experiencing severe

377   disease (7, 8), though clinical information was unknown. Furthermore, our equation relating C_t

378   values derived from a commercial diagnostic assay and SARS-CoV-2 RNA copy number means

379   that existing diagnostic test results can be converted to viral loads *without re-testing samples*.

380   While calibration of viral load measurements against all real-time RT-PCR platforms is beyond

381   our scope, this is achievable and in some cases data may already be available (23).

382   Some limitations merit mention. We only tested eight commonly-used SARS-CoV-2-

383   specific primer/probe sets, and others may exist that adapt well to RT-ddPCR. Our assay

384   performance estimates should be considered approximate, as the manufacturer-reported

385   concentration of the synthetic SARS-CoV-2 RNA standards used in our study may vary by up to

386   20% error (Twist Bioscience, personal communication). Moreover, we solely evaluated a one-

17

387 step RT-ddPCR protocol, and therefore assay performance estimates will likely differ from

388 protocols that feature independent cDNA generation followed by ddPCR. We could not precisely

389 define the upper boundary of the linear dynamic range of the E-Sarbeco, IP2 and IP4 RT-ddPCR

390 assays as linearity was maintained at the maximum input of 114,286 target copies/reaction,

391 which already exceeds the manufacturer's estimated upper range of quantification in a ddPCR

392 reaction (36). Our convenience panel of 48 SARS-CoV-2-positive diagnostic specimens also

393 likely did not capture the full range of biological variation in viral loads, though data from larger

394 cohorts (47) suggests that it was reasonably comprehensive. We also acknowledge that there is

395 measurement uncertainty with real-time RT-PCR C_t values that may subtly affect the linear

396 relationship between C_t value and RT-ddPCR-derived SARS-CoV-2 viral load described here.

397 Finally, our estimates of assay performance may not completely reflect those of the entire

398 diagnostic process, as the nucleic acid extraction step introduces additional inefficiencies.

399 In conclusion, primer/probe sets used in real-time RT-PCR-based COVID-19 diagnostic

400 tests can be migrated to RT-ddPCR to achieve SARS-CoV-2 RNA quantification with varying

401 analytical efficiency, precision and sensitivity. Of the primer/probe sets tested, the E-Sarbeco,

402 IP2 and IP4 sets performed best, where LLOQ and LLOD estimates for the E-Sarbeco assay

403 (18.6 and 4.4 copies/reaction, respectively) indicated that RT-ddPCR and real-time RT-PCR

404 have comparable sensitivity. Mathematical inference of SARS-CoV-2 copy numbers from

405 COVID-19 diagnostic test C_t values, made possible via the type of calibration performed in the

406 present study, will allow the wealth of existing diagnostic test data to be harnessed to answer

407 foundational questions in SARS-CoV-2 biology.

408

409 **Acknowledgements**

18

414

415

416   References
417
418   1.   Mellors JW, Rinaldo CR, Jr., Gupta P, White RM, Todd JA, Kingsley LA. 1996.
419   Prognosis in HIV-1 infection predicted by the quantity of virus in plasma. Science
420   272:1167-70.
421   2.   Mellors JW. 1998. Viral-load tests provide valuable answers. Sci Am 279:90-3.
422   3.   Riddler SA, Mellors JW. 1997. HIV-1 viral dynamics and viral load measurement:
423   implications for therapy. AIDS Clin Rev:47-65.
424   4.   Mellors JW, Muñoz A, Giorgi JV, Margolick JB, Tassoni CJ, Gupta P, Kingsley LA, Todd
425   JA, Saah AJ, Detels R, Phair JP, Rinaldo CR, Jr. 1997. Plasma viral load and CD4+
426   lymphocytes as prognostic markers of HIV-1 infection. Ann Intern Med 126:946-54.
427   5.   Durante-Mangoni E, Zampino R, Portella G, Adinolfi LE, Utili R, Ruggiero G. 2009.
428   Correlates and prognostic value of the first-phase hepatitis C virus RNA kinetics
429   during treatment. Clin Infect Dis 49:498-506.
430   6.   Chen G, Lin W, Shen F, Iloeje UH, London WT, Evans AA. 2006. Past HBV viral load as
431   predictor of mortality and morbidity from HCC and chronic liver disease in a
432   prospective study. Am J Gastroenterol 101:1797-803.
433   7.   Veyer D, Kernéis S, Poulet G, Wack M, Robillard N, Taly V, L'Honneur AS, Rozenberg
434   F, Laurent-Puig P, Bélec L, Hadjadj J, Terrier B, Péré H. 2020. Highly sensitive
435   quantification of plasma SARS-CoV-2 RNA shelds light on its potential clinical value.
436   Clin Infect Dis doi:10.1093/cid/ciaa1196.
437   8.   Bermejo-Martin JF, González-Rivera M, Almansa R, Micheloud D, Tedim AP,
438   Domínguez-Gil M, Resino S, Martín-Fernández M, Murua PR, Pérez-García F, Tamayo
439   L, Lopez-Izquierdo R, Bustamante E, Aldecoa C, Gómez JM, Rico-Feijoo J, Orduña A,
440   Méndez R, Fernández Natal I, Megías G, González-Estecha M, Carriedo D, Doncel C,
441   Jorge N, Ortega A, de la Fuente A, del Campo F, Fernández-Ratero JA, Trapiello W,
442   González-Jiménez P, Ruiz G, Kelvin AA, Ostadgavahi AT, Oneizat R, María Ruiz L,
443   Miguéns I, Gargallo E, Muñoz I, Pelegrin S, Martín S, García Olivares P, Cedeño JA,
444   Albi TR, Puertas C, Ángel Berezo J, Renedo G, Herrán R, Bustamante-Munguira J,
445   Enríquez P, Cicuendez R, et al. 2020. Viral RNA load in plasma is associated with
446   critical illness and a dysregulated host response in COVID-19. medRxiv
447   doi:10.1101/2020.08.25.20154252:2020.08.25.20154252.
448   9.   Han MS, Byun JH, Cho Y, Rim JH. 2020. RT-PCR for SARS-CoV-2: quantitative versus
449   qualitative. Lancet Infect Dis doi:10.1016/s1473-3099(20)30424-2.
450   10.   Liu X, Feng J, Zhang Q, Guo D, Zhang L, Suo T, Hu W, Guo M, Wang X, Huang Z, Xiong
451   Y, Chen G, Chen Y, Lan K. 2020. Analytical comparisons of SARS-COV-2 detection by
452   qRT-PCR and ddPCR with multiple primer/probe sets. Emerg Microbes Infect
453   9:1175-1179.
454   11.   Suo T, Liu X, Feng J, Guo M, Hu W, Guo D, Ullah H, Yang Y, Zhang Q, Wang X, Sajid M,
455   Huang Z, Deng L, Chen T, Liu F, Xu K, Liu Y, Zhang Q, Liu Y, Xiong Y, Chen G, Lan K,
456   Chen Y. 2020. ddPCR: a more accurate tool for SARS-CoV-2 detection in low viral
457   load specimens. Emerg Microbes Infect 9:1259-1268.
458   12.   BioRad-Laboratories-Inc. 2020. Wet-Lab Validated ddPCR Assays for Mutation
459   Detection and Copy Number Determination. https://www.bio-
460   rad.com/webroot/web/pdf/lsr/literature/Bulletin_7144.pdf. Accessed

461 13. BioRad-Laboratories-Inc. 2019. Direct Quantification of Genome Editing Efficiency
462   from Whole Cells Using SingleShot Cell Lysis Buffer and ddPCR Genome Edit
463   Detection Assays. https://www.bio-
464   rad.com/webroot/web/pdf/lsr/literature/Bulletin_7155.pdf. Accessed

465 14. Lillsunde Larsson G, Helenius G. 2017. Digital droplet PCR (ddPCR) for the detection
466   and quantification of HPV 16, 18, 33 and 45 - a short report. Cell Oncol (Dordr)
467   40:521-527.

468 15. Stevenson A, Wakeham K, Pan J, Kavanagh K, Millan D, Bell S, McLellan D, Graham
469   SV, Cuschieri K. 2020. Droplet digital PCR quantification suggests that higher viral
470   load correlates with improved survival in HPV-positive oropharyngeal tumours. J
471   Clin Virol 129:104505.

472 16. Cao WW, He DS, Chen ZJ, Zuo YZ, Chen X, Chang YL, Zhang ZG, Ye L, Shi L. 2020.
473   Development of a droplet digital PCR for detection and quantification of porcine
474   epidemic diarrhea virus. J Vet Diagn Invest 32:572-576.

475 17. Persson S, Eriksson R, Lowther J, Ellström P, Simonsson M. 2018. Comparison
476   between RT droplet digital PCR and RT real-time PCR for quantification of
477   noroviruses in oysters. Int J Food Microbiol 284:73-83.

478 18. Pinheiro-de-Oliveira TF, Fonseca AA, Jr., Camargos MF, Laguardia-Nascimento M, de
479   Oliveira AM, Cottorello ACP, Goes-Neto A, Barbosa-Stancioli EF. 2018. Development
480   of a droplet digital RT-PCR for the quantification of foot-and-mouth virus RNA. J
481   Virol Methods 259:129-134.

482 19. Bruner KM, Wang Z, Simonetti FR, Bender AM, Kwon KJ, Sengupta S, Fray EJ, Beg SA,
483   Antar AAR, Jenike KM, Bertagnolli LN, Capoferri AA, Kufera JT, Timmons A, Nobles C,
484   Gregg J, Wada N, Ho YC, Zhang H, Margolick JB, Blankson JN, Deeks SG, Bushman FD,
485   Siliciano JD, Laird GM, Siliciano RF. 2019. A quantitative approach for measuring the
486   reservoir of latent HIV-1 proviruses. Nature 566:120-125.

487 20. BioRad-Laboratories-Inc. 2020. Bio-Rad SARS-CoV-2 ddPCR Kit, Qualitative assay
488   for use in the QX200 and QXDx Droplet Digital PCR Systems Instructions for Use.

489 21. Falzone L, Musso N, Gattuso G, Bongiorno D, Palermo CI, Scalia G, Libra M, Stefani S.
490   2020. Sensitivity assessment of droplet digital PCR for SARS-CoV-2 detection. Int J
491   Mol Med 46:957-964.

492 22. de Kock R, Baselmans M, Scharnhorst V, Deiman B. 2020. Sensitive detection and
493   quantification of SARS-CoV-2 by multiplex droplet digital RT-PCR. Eur J Clin
494   Microbiol Infect Dis doi:10.1007/s10096-020-04076-3:1-7.

495 23. Yu F, Yan L, Wang N, Yang S, Wang L, Tang Y, Gao G, Wang S, Ma C, Xie R, Wang F,
496   Tan C, Zhu L, Guo Y, Zhang F. 2020. Quantitative Detection and Viral Load Analysis of
497   SARS-CoV-2 in Infected Patients. Clin Infect Dis 71:793-798.

498 24. Alteri C, Cento V, Antonello M, Colagrossi L, Merli M, Ughi N, Renica S, Matarazzo E,
499   Di Ruscio F, Tartaglione L, Colombo J, Grimaldi C, Carta S, Nava A, Costabile V,
500   Baiguera C, Campisi D, Fanti D, Vismara C, Fumagalli R, Scaglione F, Epis OM, Puoti
501   M, Perno CF. 2020. Detection and quantification of SARS-CoV-2 by droplet digital
502   PCR in real-time PCR negative nasopharyngeal swabs from suspected COVID-19
503   patients. PLoS One 15:e0236311.

504 25. Dang Y, Liu N, Tan C, Feng Y, Yuan X, Fan D, Peng Y, Jin R, Guo Y, Lou J. 2020.
505   Comparison of qualitative and quantitative analyses of COVID-19 clinical samples.
506   Clin Chim Acta 510:613-616.

507 26. World-Health-Organization. 2020. Summary of Available SARS-CoV-2 RT-PCR
508   protocols.
509 27. Corman VM, Landt O, Kaiser M, Molenkamp R, Meijer A, Chu DK, Bleicker T, Brünink
510   S, Schneider J, Schmidt ML, Mulders DG, Haagmans BL, van der Veer B, van den
511   Brink S, Wijsman L, Goderski G, Romette JL, Ellis J, Zambon M, Peiris M, Goossens H,
512   Reusken C, Koopmans MP, Drosten C. 2020. Detection of 2019 novel coronavirus
513   (2019-nCoV) by real-time RT-PCR. Euro Surveill 25.
514 28. Institut-Pasteur-Paris. 2020. Protocol: Real-time RT-PCR assays for the detection of
515   SARS-CoV-2.
516 29. Chinese-National-Institute-for-Viral-Disease-Control-and-Prevention. 2020. Specific
517   primers and probes for detection of 2019 novel coronavirus.
518 30. School-of-Public-Health-LKS-Faculty-of-Medicine-University-of-Hong-Kong. 2020.
519   Detection of 2019 novel coronavirus (2019-nCoV) in suspected human cases by RT-
520   PCR.
521 31. Centers-for-Disease-Control-and-Prevention. 2020. CDC 2019-Novel Coronavirus
522   (2019-nCoV) Real-Time RT-PCR Diagnostic Panel.
523 32. Kinloch NN, Ritchie G, Brumme CJ, Dong W, Dong W, Lawson T, Jones RB, Montaner
524   JSG, Leung V, Romney MG, Stefanovic A, Matic N, Lowe CF, Brumme ZL. 2020.
525   Suboptimal Biological Sampling as a Probable Cause of False-Negative COVID-19
526   Diagnostic Test Results. The Journal of Infectious Diseases
527   doi:10.1093/infdis/jiaa370.
528 33. Kinloch NN, Shahid A, Ritchie G, Dong W, Lawson T, Montaner JSG, Romney MG,
529   Stefanovic A, Matic N, Brumme CJ, Lowe CF, Brumme ZL, Leung V. 2020. Evaluation
530   of Nasopharyngeal Swab Collection Techniques for Nucleic Acid Recovery and
531   Participant Experience: Recommendations for COVID-19 Diagnostics. Open Forum
532   Infect Dis 7:ofaa488.
533 34. Bio-Rad-Laboratories-Inc. 2019. Droplet Digital PCR Applications Guide.
534 35. Schwaber J, Andersen S, Nielsen L. 2019. Shedding light: The importance of reverse
535   transcription efficiency standards in data interpretation. Biomol Detect Quantif
536   17:100077.
537 36. BioRad-Laboratories-Inc. 2019. Droplet Digital PCR Applications Guide.
538   https://www.bio-rad.com/webroot/web/pdf/lsr/literature/Bulletin_6407.pdf.
539   Accessed
540 37. Kim D, Lee JY, Yang JS, Kim JW, Kim VN, Chang H. 2020. The Architecture of SARS-
541   CoV-2 Transcriptome. Cell 181:914-921.e10.
542 38. Irigoyen N, Firth AE, Jones JD, Chung BY, Siddell SG, Brierley I. 2016. High-
543   Resolution Analysis of Coronavirus Gene Expression by RNA Sequencing and
544   Ribosome Profiling. PLoS Pathog 12:e1005473.
545 39. Dimmock NJ, Easton AJ, Leppard KN. 2007. Introduction to Modern Virology, 6 ed.
546   Blackwell Publishing.
547 40. Davidson AD, Williamson MK, Lewis S, Shoemark D, Carroll MW, Heesom KJ,
548   Zambon M, Ellis J, Lewis PA, Hiscox JA, Matthews DA. 2020. Characterisation of the
549   transcriptome and proteome of SARS-CoV-2 reveals a cell passage induced in-frame
550   deletion of the furin-like cleavage site from the spike glycoprotein. Genome Med
551   12:68.

552   41.   Vogels CBF, Brito AF, Wyllie AL, Fauver JR, Ott IM, Kalinich CC, Petrone ME,
553   Casanovas-Massana A, Catherine Muenker M, Moore AJ, Klein J, Lu P, Lu-Culligan A,
554   Jiang X, Kim DJ, Kudo E, Mao T, Moriyama M, Oh JE, Park A, Silva J, Song E, Takahashi
555   T, Taura M, Tokuyama M, Venkataraman A, Weizman OE, Wong P, Yang Y,
556   Cheemarla NR, White EB, Lapidus S, Earnest R, Geng B, Vijayakumar P, Odio C,
557   Fournier J, Bermejo S, Farhadian S, Dela Cruz CS, Iwasaki A, Ko AI, Landry ML,
558   Foxman EF, Grubaugh ND. 2020. Analytical sensitivity and efficiency comparisons of
559   SARS-CoV-2 RT-qPCR primer-probe sets. Nat Microbiol 5:1299-1305.
560   42.   Etievant S, Bal A, Escuret V, Brengel-Pesce K, Bouscambert M, Cheynet V, Generenaz
561   L, Oriol G, Destras G, Billaud G, Josset L, Frobert E, Morfin F, Gaymard A. 2020.
562   Performance Assessment of SARS-CoV-2 PCR Assays Developed by WHO Referral
563   Laboratories. J Clin Med 9.
564   43.   Bustin SA, Benes V, Nolan T, Pfaffl MW. 2005. Quantitative real-time RT-PCR--a
565   perspective. J Mol Endocrinol 34:597-601.
566   44.   Sanders R, Mason DJ, Foy CA, Huggett JF. 2013. Evaluation of digital PCR for absolute
567   RNA quantification. PLoS One 8:e75296.
568   45.   Levesque-Sergerie JP, Duquette M, Thibault C, Delbecchi L, Bissonnette N. 2007.
569   Detection limits of several commercial reverse transcriptase enzymes: impact on the
570   low- and high-abundance transcript levels assessed by quantitative RT-PCR. BMC
571   Mol Biol 8:93.
572   46.   Lai CC, Wang CY, Ko WC, Hsueh PR. 2020. In vitro diagnostics of coronavirus disease
573   2019: Technologies and application. J Microbiol Immunol Infect
574   doi:10.1016/j.jmii.2020.05.016.
575   47.   Jacot D, Greub G, Jaton K, Opota O. 2020. Viral load of SARS-CoV-2 across patients
576   and compared to other respiratory viruses. Microbes Infect
577   doi:10.1016/j.micinf.2020.08.004.
578   48.   Pan Y, Zhang D, Yang P, Poon LLM, Wang Q. 2020. Viral load of SARS-CoV-2 in
579   clinical samples. Lancet Infect Dis 20:411-412.
580   49.   Zou L, Ruan F, Huang M, Liang L, Huang H, Hong Z, Yu J, Kang M, Song Y, Xia J, Guo Q,
581   Song T, He J, Yen HL, Peiris M, Wu J. 2020. SARS-CoV-2 Viral Load in Upper
582   Respiratory Specimens of Infected Patients. N Engl J Med 382:1177-1179.
583   50.   Huang Y, Chen S, Yang Z, Guan W, Liu D, Lin Z, Zhang Y, Xu Z, Liu X, Li Y. 2020. SARS-
584   CoV-2 Viral Load in Clinical Samples from Critically Ill Patients. Am J Respir Crit Care
585   Med 201:1435-1438.
586

Source	Name	Gene Target	Primer/ Probe	Sequence[φ] (5'-> 3')	Coordinates[ψ]
Charité-Berlin	E-Sarbeco	E	Fwd Primer	ACAGGTACGTTAATAGTTAATAGCGT	26,269- 26,294
			Rev Primer	ATATTGCAGCAGTACGCACACA	26,381- 26,360
			Probe	FAM-ACACTAGCC/ZEN/ATCCTTACTGCGCTTCG-3IABkFQ	26,332- 26,357
Pasteur Institute	IP2	ORF1a	Fwd Primer	ATGAGCTTAGTCCTGTTG	12,690- 12,707
			Rev Primer	CTCCCTTTGTTGTGTTGT	12,797- 12,780
			Probe	HEX-AGATGTCTT/ZEN/GTGCTGCCGGTA-3IABkFQ	12,717- 12,737
	IP4	ORF1b	Fwd Primer	GGTAACTGGTATGATTTCG	14,080- 14,098
			Rev Primer	CTGGTCAAGGTTAATATAGG	14,105- 14,123
			Probe	FAM-TCATACAAA/ZEN/CCACGCCAGG-3IABkFQ	14,186- 14,167
China CDC	China-ORF	ORF1a	Fwd Primer	CCCTGTGGGTTTTACACTTAA	13,342- 13,362
			Rev Primer	ACGATTGTGCATCAGCTGA	13,460- 13,442
			Probe	FAM-CCGTCTGCG/ZEN/GTATGTGGAAAGGTTATGG-3IABkFQ	13,377- 13,404
	China-N	N	Fwd Primer	GGGGAACTTCTCCTGCTAGAAT	28,881- 28,902
			Rev Primer	CAGACATTTTGCTCTCAAGCTG	28,979- 28,958
			Probe	FAM-TTGCTGCTG/ZEN/CTTGACAGATT-3IABkFQ	28,934- 28,953
Hong Kong University	HKU-ORF	ORF1b	Fwd Primer	TGGGGYTTTACRGGTAACCT	18,778- 18,797
			Rev Primer	AACRCGCTTAACAAAGCACTC	18,849- 18,872
			Probe	FAM-TAGTTGTGA/ZEN/TGCWATCATGACTAG-3IABkFQ	18,909- 18,889
	HKU-N	N	Fwd Primer	TAATCAGACAAGGAACTGATTA	29,145- 29,166
			Rev Primer	CGAAGGTGTGACTTCCATG	29,179- 29,198
			Probe	FAM-GCAAATTGT/ZEN/GCAATTTGCGG-3IABkFQ	29,254- 29,236
US CDC	US-CDC-N1	N	Fwd Primer	GACCCCAAAATCAGCGAAAT	28,287- 28,306
			Rev Primer	TCTGGTTACTGCCAGTTGAATCTG	28,358- 28,335
			Probe	FAM-ACCCCGCAT/ZEN/TACGTTTGGTGGACC-3IABkFQ	28,309- 28,332

[φ] FAM= 6-Carboxyfluorescein; HEX= Hexachloro-Fluorescein; ZEN= internal ZEN quencher (Integrated DNA Technologies); 3IABkFQ= 3' Iowa Black Black Hole Quencher (Integrated DNA Technologies)

[ψ] Coordinates based on the SARS-CoV-2 Wuhan-Hu-1 genome (Genbank Accession Number: MN908947.3)

Figure 1: Thermal cycling optimization (A). RT-ddPCR plots for annealing/extension under a 50-63°C thermal gradient for the E-Sarbeco primer/probe set. A representative RT-ddPCR plot for a no template control (NTC) which only included non-target DNA/RNA (see methods) at the temperature used in subsequent experiments, is also shown. Positive droplets (blue) are above the threshold (pink line); negative droplets (grey) are below the line. Colored boxes below each well indicate if results met standards for inclusion (green) or not (red) (see methods). (B). Same as panel A, but for HKU-ORF primer/probe set. (C). Acceptable RT and annealing/extension temperature ranges for each primer/probe set.

Figure 2: Analytical efficiency and precision of primer/probe sets. (A) Analytical efficiency of each primer/probe set, calculated as the measured divided by the input SARS-CoV-2 RNA copies multiplied by 100%, is shown for reactions containing 1,000 and 100 input copies of synthetic SARS-CoV-2 RNA. Bars represent 95% Total Poisson Confidence Intervals. **(B).** Precision of each primer/probe set, defined as the coefficient of variation (expressed as a percentage, CV%) of measured copies, is shown for reactions containing 1,000 and 100 input copies of synthetic SARS-CoV-2 RNA. (C). Plotting precision versus analytical efficiency at 1,000 input SARS-CoV-2 RNA copies identifies E-Sarbeco, IP2 and IP4 primer/probe sets as having analytical efficiencies >50% and CV (%) <15%. (D). Same as C, but for 100 input SARS-CoV-2 RNA copies.

Figure 3: Linear Dynamic Range (LDR) of E-Sarbeco, IP2 and IP4 RT-ddPCR assays. (A). left: log_{10}Measured SARS-CoV-2 RNA copies over serial dilutions of synthetic SARS-CoV-2 RNA standards ranging from 114,286 to 2.32 copies/reaction (shown as log_{10} values), using the

25

E-Sarbeco primer/probe set. Error bars indicate 95% Total Poisson Confidence Intervals for two merged replicates, where in some cases error bars are too small to visualize. The regression line joins all data points included in the LDR, where the lower boundary of the LDR represents the lower limit of quantification (LLOQ) of the assay. Data points that yielded undetectable measurements are set arbitrarily to -0.35log$_{10}$Measured copies/reaction for visualization. right: Log$_{10}$Residuals, calculated as log$_{10}$Measured SARS-CoV-2 RNA copies/reaction minus log$_{10}$Calulated SARS-CoV-2 RNA copies/reaction from the LDR regression. Grey shading indicates data points outside the LDR. Residuals for data points that yielded undetectable measurements are arbitrarily set to -0.4 for visualization. (B). Same as A, but for the IP2 primer/probe set (C). Same as A, but for the IP4 primer/probe set.

Figure 4: Lower Limit of Detection (LLOD) of the E-Sarbeco, IP2 and IP4 RT-ddPCR assays. (A). The probability of detecting SARS-CoV-2 RNA (%) in 1:2 in serial dilutions of synthetic SARS-CoV-2 RNA from 47.6 to 0.74 input copies/reaction using the E-Sarbeco primer/probe set is analyzed using probit regression (solid black line; dashed line denotes the 95% confidence interval). The LLOD, defined as the concentration of SARS-CoV-2 RNA in a reaction where the probability of detection in the assay was 95%, was interpolated from the standard curve and is shown as a colored dashed line (B). Same as A, but for the IP2 primer/probe set (C). Same as A, but for the IP4 primer/probe set.

Figure 5: Log$_{10}$SARS-CoV-2 RNA loads in diagnostic specimens (A). SARS-CoV-2 E (green circles), ORF1a (red squares) and ORF1b (blue triangles) gene copy numbers, expressed as RNA copies/μl of nucleic acid extract. Line and bars indicate median and interquartile range,

26

respectively. **(B)** Correlation between Log_{10}SARS-CoV-2 E and ORF1a gene RNA copies/µl extract. (C). Correlation between Log_{10}SARS-CoV-2 E and ORF1b gene RNA copies/µl extract. (D) Correlation and Concordance between Log_{10}SARS-CoV-2 ORF1a and ORF1b gene RNA copies/µl extract.

Figure 6: Relationship between SARS-CoV-2 RNA copies equivalent and diagnostic test C_t value. C_t value, determined using the LightMix® 2019-nCoV real-time RT-PCR assay (E-gene target) is plotted against log_{10}SARS-CoV-2 E gene RNA copies equivalent, which represents the number of SARS-CoV-2 RNA copies measured by RT-ddPCR in 9µl extract (the template volume in the LightMix® assay). The linear regression (solid black line) transitions to a dashed line below the LLOQ.

Supplementary Figure 1: All experiments using synthetic SARS-CoV-2 synthetic standards were performed in a consistent background of human nucleic acids to mimic a real human sample. Example experiment showing consistent levels of background human cells/µl extract (determined by dividing measured human RPP30 DNA copy number by two; black triangles), and human RNAse P RNA levels (grey squares) across a titration of SARS-CoV-2 synthetic RNA standards, measured using the E-Sarbeco primer/probe set (green circles). Error bars indicate 95% Total Poisson Confidence Intervals for two merged replicates, where in some cases error bars are too small to visualize. Grey (RNase P) and black (RPP30) dashed lines indicate copies measured control experiments lacking SARS-CoV-2 RNA.

Supplementary Figure 2: Duplexing the IP2 and IP4 primer/probe sets reduces analytical efficiency and precision. (A). Analytical efficiency of SARS-CoV-2 quantification was evaluated for the IP2 and IP4 primer/probe sets when used in separate reactions (dark red and dark blue, respectively) and when duplexed (light red and light blue, respectively), in reactions containing 1,000 and 100 viral RNA input copies. Error bars represent 95% Total Poisson Confidence Intervals. (B). Same as A, but for assay precision (coefficient of variation, CV%).

Supplementary Figure 3: Log$_{10}$SARS-CoV-2 RNA loads in diagnostic specimens, normalized to human cells sampled. (A) SARS-CoV-2 E (green circles), ORF1a (red squares) and ORF1b (blue triangles) gene copy numbers, expressed as RNA copies/1,000 human cells. Line and bars indicate median and interquartile range, respectively. (B) Correlation between SARS-CoV-2 RNA copies/μl extract and RNA copies/1,000 human cells.

Supplemental Figure 4: Residuals of relationship between SARS-CoV-2 RNA copies equivalent and diagnostic test C$_t$ value. Log$_{10}$Residuals are calculated as log$_{10}$Measured SARS-CoV-2 RNA copies equivalent minus log$_{10}$Calulated SARS-CoV-2 RNA copies equivalent from the regression line shown in Figure 6.

Supplemental Figure 5: Relationship between SARS-CoV-2 RNA copies/1,000 human cells and C$_t$ value. Same data as shown in Figure 6, but where the measured SARS-CoV-2 RNA copies/μl extract were normalized to copies/1,000 human cells. The linear regression is shown as a solid black line.

28

A E-Sarbeco Annealing/Extension
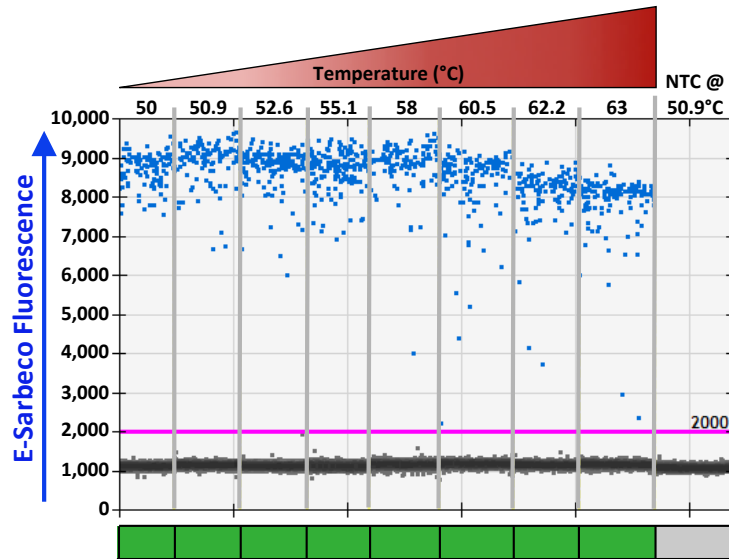
B HKU-ORF Annealing/Extension
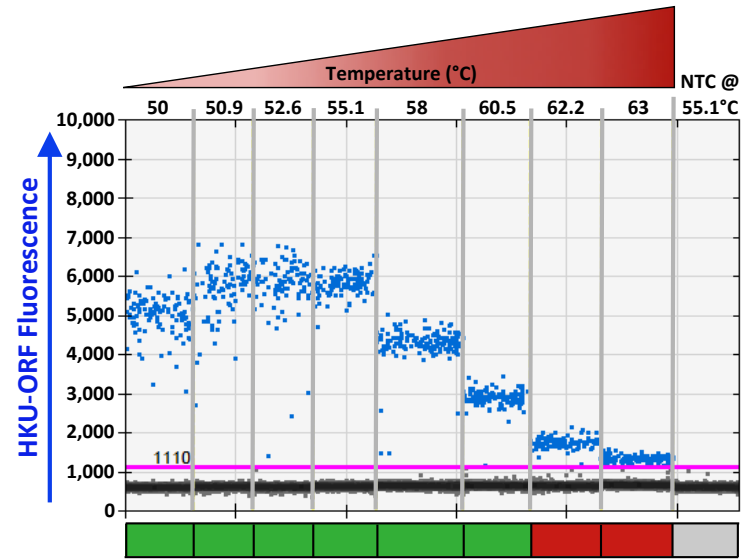
C

Acceptable Temperature °C	E-Sarbeco	IP2	IP4	CHINA-ORF	CHINA-N	HKU-ORF	HKU-N	US-CDC-N1
RT	42- 49.7	42- 51.5	42- 50.9	42- 51.5	42.7- 50.9	42- 51.5	42- 51.5	42- 45.7
Annealing/ Extension	50- 63	50- 60.5	50- 60.5	50- 63	50- 60.5	50- 60.5	50.9- 60.5	50- 63

Figure 1: Thermal cycling optimization (A). RT-ddPCR plots for annealing/extension under a 50-63°C thermal gradient for the E-Sarbeco primer/probe set. A representative RT-ddPCR plot for a no template control (NTC) which only included non-target DNA/RNA (see methods) at the temperature used in subsequent experiments, is also shown. Positive droplets (blue) are above the threshold (pink line); negative droplets (grey) are below the line. Colored boxes below each well indicate if results met standards for inclusion (green) or not (red) (see methods). (B). Same as panel A, but for HKU-ORF primer/probe set. (C). Acceptable RT and annealing/extension temperature ranges for each primer/probe set.

Figure 2: Analytical efficiency and precision of primer/probe sets. (A) Analytical efficiency of each primer/probe set, calculated as the measured divided by the input SARS-CoV-2 RNA copies multiplied by 100%, is shown for reactions containing 1,000 and 100 input copies of synthetic SARS-CoV-2 RNA. Bars represent 95% Total Poisson Confidence Intervals. **(B).** Precision of each primer/probe set, defined as the coefficient of variation (expressed as a percentage, CV%) of measured copies, is shown for reactions containing 1,000 and 100 input copies of synthetic SARS-CoV-2 RNA. (C). Plotting precision versus analytical efficiency at 1,000 input SARS-CoV-2 RNA copies identifies E-Sarbeco, IP2 and IP4 primer/probe sets as having analytical efficiencies >50% and CV (%) <15%. (D). Same as C, but for 100 input SARS-CoV-2 RNA copies.

A E-Sarbeco

R²= 0.99951
LDR= 18.6- 114,286 SARS-CoV-2 E gene RNA input copies/ reaction

B IP2

R²= 0.9995
LDR= 18.6- 114,286 SARS-CoV-2 ORF1a gene RNA input copies/ reaction

C IP4

R²= 0.9975
LDR= 37.2- 114,286 SARS-CoV-2 ORF1b gene RNA input copies/ reaction

log_{10}Meaured SARS-CoV-2 RNA Copies/ Reaction

log_{10}Input SARS-CoV-2 RNA Copies/ Reaction

log_{10}Residuals
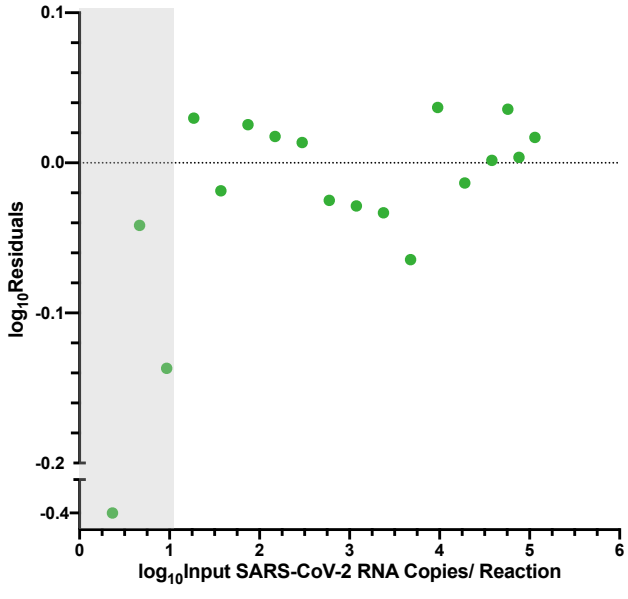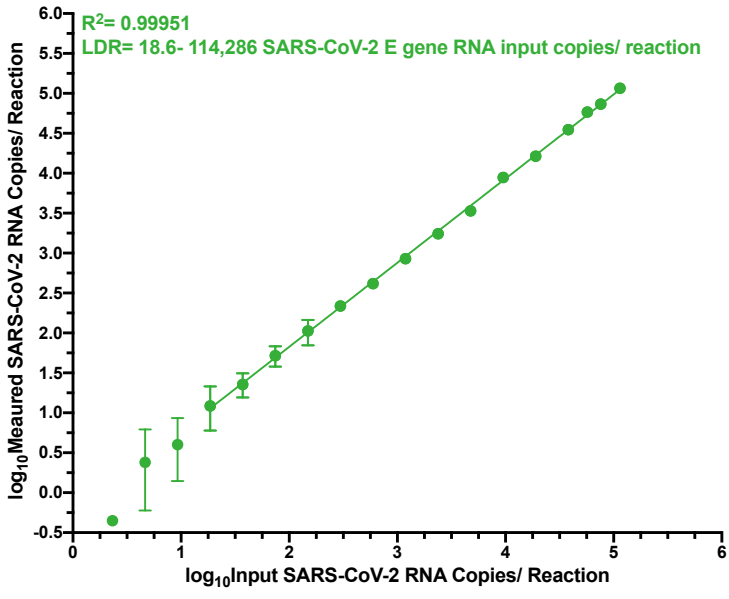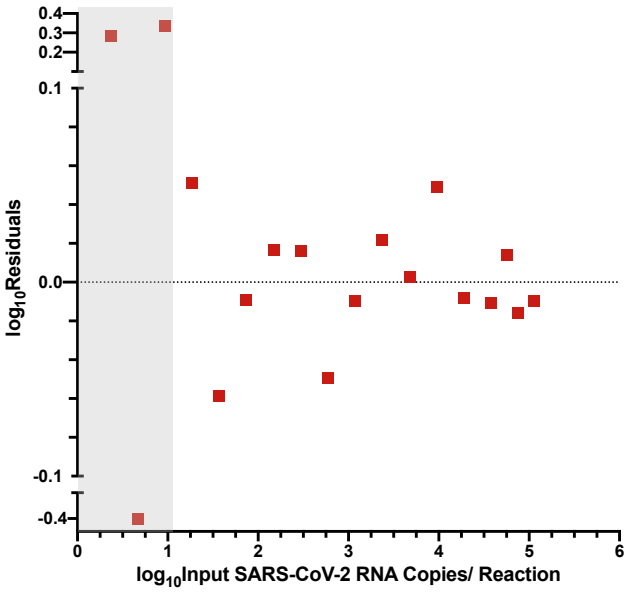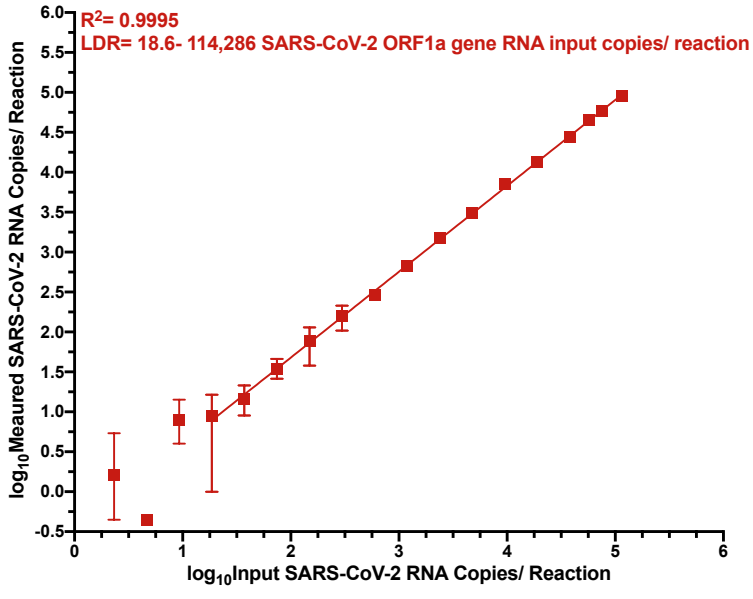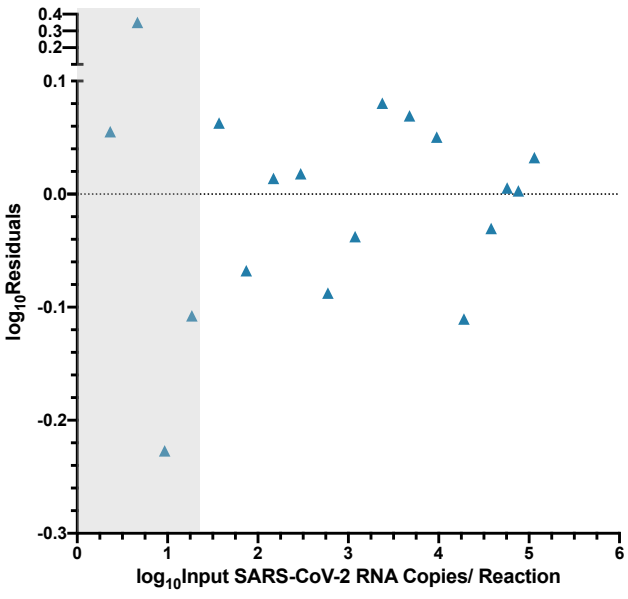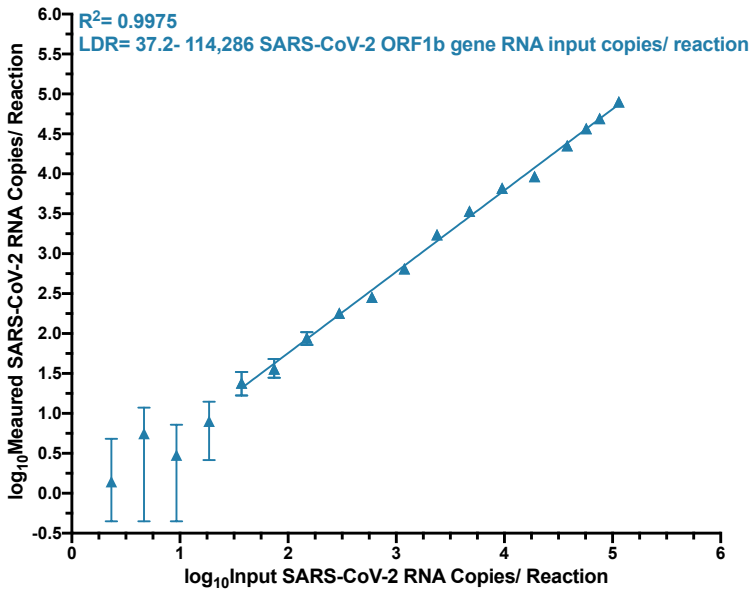
Figure 3: Linear Dynamic Range (LDR) of E-Sarbeco, IP2 and IP4 RT-ddPCR assays. (A). left: $\log_{10}$Measured SARS-CoV-2 RNA copies over serial dilutions of synthetic SARS-CoV-2 RNA standards ranging from 114,286 to 2.32 copies/reaction (shown as $\log_{10}$ values), using the E-Sarbeco primer/probe set. Error bars indicate 95% Total Poisson Confidence Intervals for two merged replicates, where in some cases error bars are too small to visualize. The regression line joins all data points included in the LDR, where the lower boundary of the LDR represents the lower limit of quantification (LLOQ) of the assay. Data points that yielded undetectable measurements are set arbitrarily to -0.35$\log_{10}$Measured copies/reaction for visualization. right: $\log_{10}$Residuals, calculated as $\log_{10}$Measured SARS-CoV-2 RNA copies/reaction minus $\log_{10}$Calulated SARS-CoV-2 RNA copies/reaction from the LDR regression. Grey shading indicates data points outside the LDR. Residuals for data points that yielded undetectable measurements are arbitrarily set to -0.4 for visualization. (B). Same as A, but for the IP2 primer/probe set (C). Same as A, but for the IP4 primer/probe set.
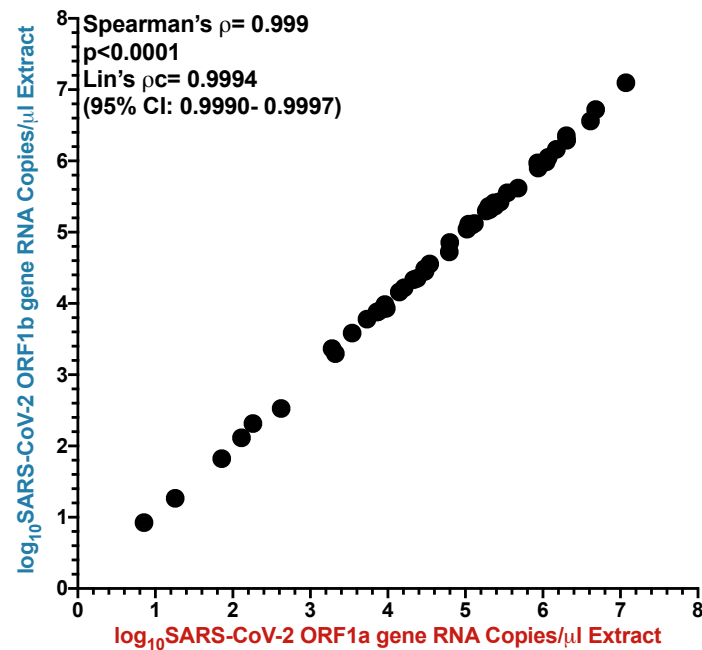
A E-Sarbeco

LLOD= 4.4 (95% CI: 2.4- 5.7) SARS-CoV-2 E gene RNA copies/reaction

B IP2

LLOD= 7.8 (95% CI: 4.4- 10.3) SARS-CoV-2 ORF1a gene RNA copies/reaction

C IP4

LLOD= 12.6 (95% CI: 6.9- 16.5) SARS-CoV-2 ORF1b gene RNA copies/reaction

Figure 4: Lower Limit of Detection (LLOD) of the E-Sarbeco, IP2 and IP4 RT-ddPCR assays. (A). The probability of detecting SARS-CoV-2 RNA (%) in 1:2 in serial dilutions of synthetic SARS-CoV-2 RNA from 47.6 to 0.74 input copies/reaction using the E-Sarbeco primer/probe set is analyzed using probit regression (solid black line; dashed line denotes the 95% confidence interval). The LLOD, defined as the concentration of SARS-CoV-2 RNA in a reaction where the probability of detection in the assay was 95%, was interpolated from the standard curve and is shown as a colored dashed line (B). Same as A, but for the IP2 primer/probe set (C). Same as A, but for the IP4 primer/probe set.

A

B Spearman's $\rho = 0.9949$
p<0.0001

C Spearman's $\rho = 0.9951$
p<0.0001

D Spearman's $\rho = 0.999$
p<0.0001
Lin's $\rho c = 0.9994$
(95% CI: 0.9990- 0.9997)

Figure 5: Log$_{10}$SARS-CoV-2 RNA loads in diagnostic specimens (A). SARS-CoV-2 E (green circles), ORF1a (red squares) and ORF1b (blue triangles) gene copy numbers, expressed as RNA copies/µl of nucleic acid extract. Line and bars indicate median and interquartile range, respectively. **(B)** Correlation between Log$_{10}$SARS-CoV-2 E and ORF1a gene RNA copies/µl extract. (C). Correlation between Log$_{10}$SARS-CoV-2 E and ORF1b gene RNA copies/µl extract. (D) Correlation and Concordance between Log$_{10}$SARS-CoV-2 ORF1a and ORF1b gene RNA copies/µl extract.

$R^2 = 0.99901$

$\log_{10}$SARS-CoV-2 E-gene RNA Copies Equivalent$= -0.3038(C_t) + 11.7$

Figure 6: Relationship between SARS-CoV-2 RNA copies equivalent and diagnostic test C_t value. C_t value, determined using the LightMix® 2019-nCoV real-time RT-PCR assay (E-gene target) is plotted against $\log_{10}$SARS-CoV-2 E gene RNA copies equivalent, which represents the number of SARS-CoV-2 RNA copies measured by RT-ddPCR in 9μl extract (the template volume in the LightMix® assay). The linear regression (solid black line) transitions to a dashed line below the LLOQ.
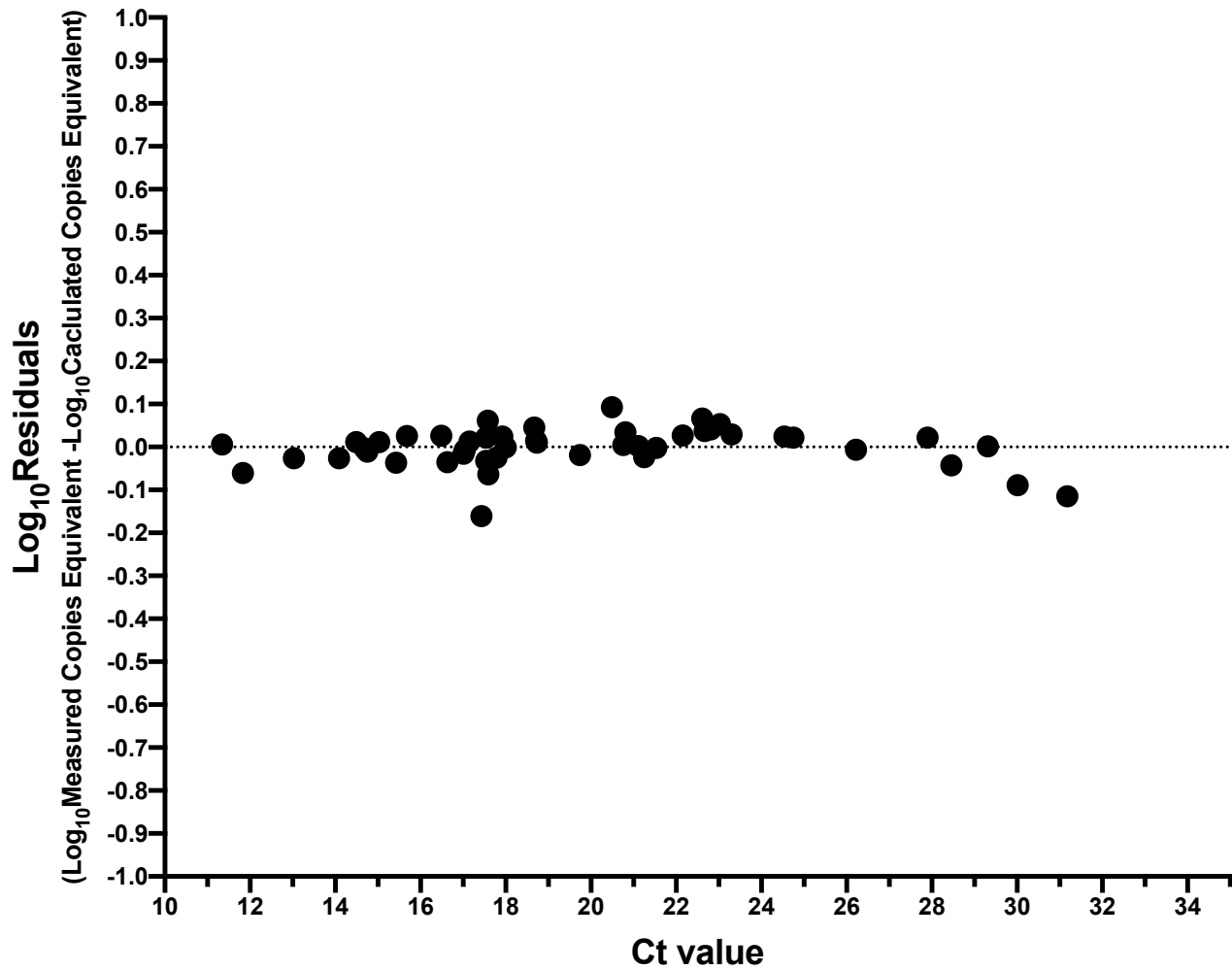
Supplementary Figure 1: All experiments using synthetic SARS-CoV-2 synthetic standards were performed in a consistent background of human nucleic acids to mimic a real human sample. Example experiment showing consistent levels of background human cells/µl extract (determined by dividing measured human RPP30 DNA copy number by two; black triangles), and human RNAse P RNA levels (grey squares) across a titration of SARS-CoV-2 synthetic RNA standards, measured using the E-Sarbeco primer/probe set (green circles). Error bars indicate 95% Total Poisson Confidence Intervals for two merged replicates, where in some cases error bars are too small to visualize. Grey (RNase P) and black (RPP30) dashed lines indicate copies measured control experiments lacking SARS-CoV-2 RNA.
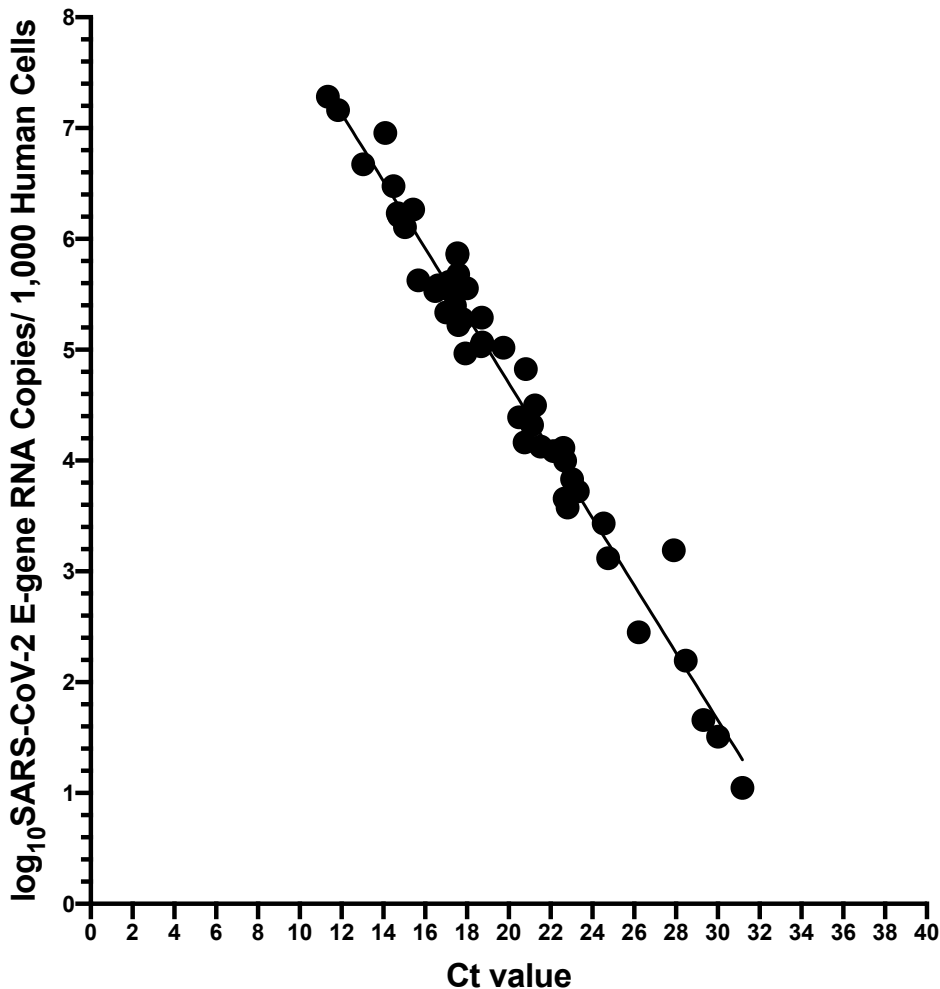
Supplementary Figure 2: Duplexing the IP2 and IP4 primer/probe sets reduces analytical efficiency and precision. (A). Analytical efficiency of SARS-CoV-2 quantification was evaluated for the IP2 and IP4 primer/probe sets when used in separate reactions (dark red and dark blue, respectively) and when duplexed (light red and light blue, respectively), in reactions containing 1,000 and 100 viral RNA input copies. Error bars represent 95% Total Poisson Confidence Intervals. (B). Same as A, but for assay precision (coefficient of variation, CV%).

Supplementary Figure 3: Log$_{10}$SARS-CoV-2 RNA loads in diagnostic specimens, normalized to human cells sampled. (A) SARS-CoV-2 E (green circles), ORF1a (red squares) and ORF1b (blue triangles) gene copy numbers, expressed as RNA copies/1,000 human cells. Line and bars indicate median and interquartile range, respectively. **(B)** Correlation between SARS-CoV-2 RNA copies/µl extract and RNA copies/1,000 human cells.

Supplemental Figure 4: Residuals of relationship between SARS-CoV-2 RNA copies equivalent and diagnostic test C_t value. Log_{10}Residuals are calculated as log_{10}Measured SARS-CoV-2 RNA copies equivalent minus log_{10}Calulated SARS-CoV-2 RNA copies equivalent from the regression line shown in Figure 6.

$R^2= 0.97079$

log_{10}SARS-CoV-2 E-gene RNA Copies/1,000 Human Cells$= -0.3041(C_t) + 10.8$

Supplemental Figure 5: Relationship between SARS-CoV-2 RNA copies/1,000 human cells and C_t value. Same data as shown in Figure 6, but where the measured SARS-CoV-2 RNA copies/µl extract were normalized to copies/1,000 human cells. The linear regression is shown as a solid black line.